

# Suppression of a Nonpremixed Flame Stabilized by a Backward-Facing Step

FUMIAKI TAKAHASHI,\* W. JOHN SCHMOLL, and EDWARD A. STRADER

*University of Dayton Research Institute, 300 College Park, Dayton, OH 45469, USA*

VINCENT M. BELOVICH

*Air Force Research Laboratory, Wright-Patterson Air Force Base, OH 45433, USA*

The stabilization and suppression behavior of a nonpremixed methane flame formed behind a backward-facing step in a combustion tunnel has been studied by impulsively injecting a gaseous fire-extinguishing agent ( $\text{CF}_3\text{Br}$ ) into the airflow. Optical observations, including a schlieren method, revealed that two distinct flame stabilization and suppression regimes, i.e., (I) rim-attached and (II) wake-stabilized, appeared as the mean air velocity was increased. The suppression in regime I occurred after immediate detachment of the flame at agent arrival, followed by blowout of the flame in the shear layer downstream. The suppression in regime II took place as a result of consecutive extinction of the flames in the shear layer and the recirculation zone, and the latter flame is controlling. The characteristic mixing (or residence) time in the recirculation zone, measured by the sodium D-line emission method, linearly depended on a simple similarity parameter, i.e., the step height divided by the effective mean air velocity. For long agent injection periods, the critical agent mole fraction at suppression approached a minimum value of  $\sim 0.025$ , which was identical to the value obtained using a counterflow diffusion flame. On the other hand, the critical agent mole fraction at suppression increased dramatically as the agent injection period was decreased below the characteristic mixing time. Under relatively high air velocities (regime II), the critical agent mole fraction at suppression normalized by the minimum value was a unique function of the agent injection period normalized by the characteristic mixing time and can be predicted using a theoretical expression. Furthermore, the total agent mass delivered can be minimized at the injection period near the characteristic mixing time. Published by Elsevier Science Inc.

## INTRODUCTION

Because of its superior effectiveness, halon 1301 (bromotrifluoromethane,  $\text{CF}_3\text{Br}$ ) has been used as a fire-extinguishing agent to protect aircraft, ships, vehicles, and facilities. However, due to its high ozone-depletion potential, halon 1301 was banned from production in 1994 [1]. As halon 1301 is replaced with a possibly less effective agent, the amount of replacement agent required for fire suppression over a range of operating conditions must be determined. In complex geometries, flame stability may be a dominant factor affecting fire suppression. An obstruction such as a baffle plate, bluff body, or backward-facing step in an airflow can enhance the stability of both premixed [2] and diffusion flames [3, 4]. A recirculation zone behind the obstruction provides conditions favorable for

flame holding, i.e., lower velocities, heat recycling to the flame stabilizing region, augmented heat transfer to condensed fuel surfaces, and enhanced mixing of fuel, air, and hot combustion products. Thus, clutter in the aircraft engine nacelle, which is ventilated to prevent the build-up of combustible vapors, can affect the behavior of fires and the performance of fire suppression agents [5–11]. The fuel sources are leaking jet-fuel and hydraulic-fluid lines that can feed the fire in the form of a spray or pool. Similar conditions may exist in fires in aircraft dry bays, shipboard machinery space, or ground armored vehicle compartments. Suppression occurs when the concentration of fire-extinguishing agent reaches a critical value in the fire zone. After the fire is extinguished, reignition may occur as the fuel-air mixture makes contact with hot metal surfaces or sparks from damaged electrical circuits.

It is not clear whether the flame extinguishing data obtained by conventional cup-burner or counterflow-diffusion-flame methods [12–18] can characterize the flames stabilized by an obstruction. Few results have been reported in

\*Corresponding author. Current address: National Center for Microgravity Research on Fluids and Combustion, NASA Glenn Research Center, MS 500-115, 21000 Brookpark Road, Cleveland, OH 44135. E-mail: Fumiaki.Takahashi@grc.nasa.gov

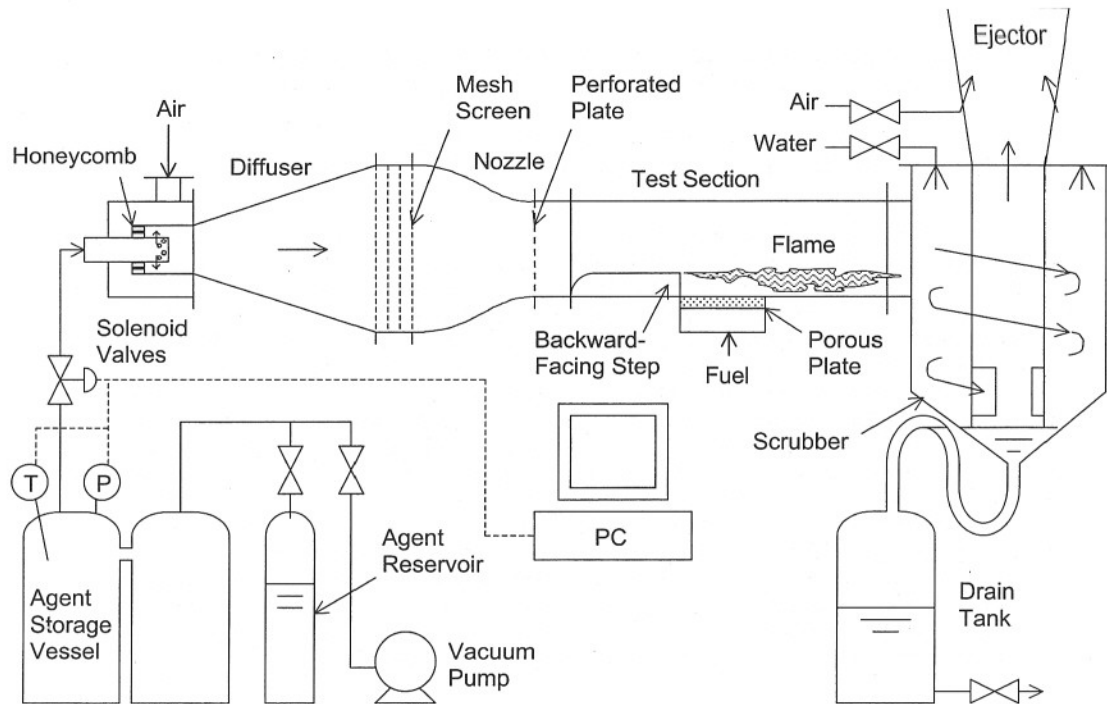


Fig. 1. Experimental apparatus.

the literature on the suppression of obstruction-stabilized nonpremixed flames. The suppression of baffle-stabilized kerosene pool fires in a wind tunnel was studied [5–8] using nitrogen and methylbromide ( $\text{CH}_3\text{Br}$ ) as the fire-extinguishing agents, and the critical agent concentration at extinguishment was reported as a function of the air velocity. It was concluded [5] that the most stable type of flame to be encountered in an aircraft engine fire is a liquid surface diffusion flame from a pool of fuel burning behind an obstruction in an airflow. By using an axisymmetric baffle-stabilized spray flame and various halogenated agents, Hamins et al. [19] identified two crucial parameters: a characteristic mixing time that describes the rate of agent entrainment into the recirculation zone and the critical agent concentration at suppression for long agent injection durations. Hamins et al. derived an expression for the critical agent mole fraction as a function of the injection duration and fitted the experimental data by adjusting the characteristic mixing time as a parameter.

The objective of this study is to gain a better understanding of the flame stabilization and suppression behavior of step-stabilized nonpre-

mixed flames. Methane and halon 1301 were used to obtain baseline suppression-limit data to extract a physical insight into underlying mechanisms common in obstruction-stabilized pool flames. In particular, the characteristic mixing (residence) time in the recirculation zone was measured for the first time and correlated with an experimental similarity parameter in an attempt to obtain a universal suppression-limit curve.

## EXPERIMENTAL TECHNIQUES

The experimental apparatus (Fig. 1) consists of the fuel, air, and agent supply systems, a horizontal small-scale combustion tunnel ( $154 \times 154 \text{ mm}^2$  cross-section, 77 cm length), and a scrubber. Methane issues upward at a mean velocity of 0.7 cm/s (22-W heat release) from a water-cooled porous plate ( $150 \text{ mm} \times 150 \text{ mm} \times 12.7 \text{ mm}$  thickness, 316L stainless steel) placed flush with the bottom surface of the test section downstream of an obstruction. Figure 2 shows schematics of the obstruction used: a baffle plate (height  $h_s = 64 \text{ mm}$ ), a J-flange

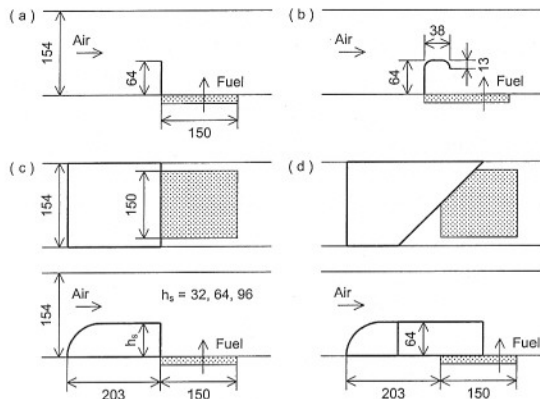


Fig. 2. Schematics of the obstruction. (a) Baffle plate, (b) J-flange, (c) backward-facing step, and (d) 45°-angle step.

( $h_s = 64$  mm), a backward-facing step ( $h_s = 32$  mm, 64 mm, or 96 mm), and a 45°-angle step ( $h_s = 64$  mm). The airflow is conditioned by passing through honeycombs, a diffuser, mesh screens (#100), a contoured contraction nozzle, and a turbulence-generating perforated plate (33% opening, 2.4-mm-dia. holes). The turbulence level in the combustion tunnel is up to ~6%. The mean air velocities at the test section inlet ( $U_{a0}$ ) and the step ( $U_{as}$ ) are calculated by dividing the volumetric flow rate by the cross-sectional areas of the full test section and the air passage above the step, respectively. Hence,  $U_{as} = [1/(1 - h_s/h_T)]U_{a0}$ , where  $h_T$  (0.154 m) is the total height of the test section. The effective mean air velocity is then calculated as  $U_a^* = (U_{a0} + U_{as})/2$ . Table 1 shows  $U_{a0}$ ,  $U_{as}$ , and  $U_a^*$  for the three step heights under typical experimental conditions.

The agent supply system, which is similar to that of Hamins et al. [11, 13, 19], consists of a (liquid) agent reservoir (3.8 L), two connected gaseous agent storage vessels (38 L each), and

up to four computer-controlled solenoid valves (Peter Paul, 9.5-mm orifice, ~12-ms response time) that are connected in parallel. The gaseous agent was injected impulsively into the airflow ~1 m upstream of the flame. Uniform agent dispersion into the airstream was achieved by injecting the agent perpendicular to the airflow in a reduced-diameter (108 mm) section through  $16 \times 6.4$ -mm-dia. holes in two rows in a 25.4-mm-o.d. closed-end tube. The mesh screens and a perforated plate downstream enhance further mixing. The schlieren visualization, to be described later, revealed fairly good agent dispersion and mixing in air. The agent storage volume, including two storage vessels and associated plumbing, is 80.4 L. The agent temperature and pressure in the second storage vessel are measured with a type-T (copper-constantan) thermocouple and a pressure transducer. The amount of injected agent is controlled by varying the initial storage vessel pressure and the time period that the valve is open and is determined from the difference between the initial and final pressures and temperatures in the storage vessel using the ideal-gas equation of state. Because the sufficiently large storage volume results in a relatively small pressure drop during agent discharge and the valve response time is relatively short compared to the agent injection period, a constant agent discharge rate is assumed. Therefore, the mean volumetric agent concentration is determined by dividing the mean agent flow rate ([volume]/[injection period]) by the total flow rate.

A uniquely designed cyclone-type scrubber is attached to the exit of the test section to remove acidic gases (HF) by water sprays from eight

TABLE 1  
Air Flow Conditions

$U_{a0}$ (m/s)	$h_s = 32$ mm		$h_s = 64$ mm		$h_s = 96$ mm	
	$U_{as}$ (m/s)	$U_a^*$ (m/s)	$U_{as}$ (m/s)	$U_a^*$ (m/s)	$U_{as}$ (m/s)	$U_a^*$ (m/s)
0.29	0.36	0.33	0.49	0.39	0.76	0.53
1.4	1.8	1.6	2.5	2.0	3.8	2.6
2.9	3.6	3.2	4.9	3.9	7.6	5.2
7.1	9.0	8.1	12.2	9.6	18.9	13.0
10.8	13.6	12.2	18.4	14.6	28.6	19.7

pressure-swirl atomizers (Delavan, nominal 15-gallon/in flow rate, 90° solid cone spray) on the top plate. The gases are exhausted through the central tube and the water is collected in a drain tank. An air-driven ejector (7.6-cm inlet diameter, 18.5-cm outlet diameter, 84-cm length) is attached to the scrubber exit to reduce the backpressure and adjust the pressure of the test section equal to atmospheric.

A schlieren deflectometry system used for optical observations consists of a xenon flashlamp (EG&G FX-198, 1- $\mu$ s duration, 5-J maximum energy per flash), concave mirrors (15-cm dia., f10), a knife-edge, and a camera. The flashlamp is synchronized with a free-running color video camera (Panasonic GP-US502, 12.5–75-mm f.l.) at 60 Hz or a 35-mm SLR camera (Nikon FM-2, 200-mm f.l.) set at a known time delay after activating the agent release valve. The images are recorded using an S-VHS recorder (Sony SVO-2000) or on 35-mm color slide film (Kodak EPH-1600).

The suppression-limit experiment is conducted using a right-angle backward-facing step as follows. First, a stable flame is established for a fixed air velocity for a period of at least 20 min, and then the agent is injected for a particular storage vessel pressure and an injection period to determine whether or not the flame extinguishes. The agent injection test is repeated 20 times and the probability of suppression is determined by dividing the number of extinguishments by the total number of runs. Then either the storage vessel pressure (which determines agent concentration) or injection period is varied step-wise and the experiment is repeated. The suppression condition is confirmed at a probability of 90% chosen arbitrarily.

The characteristic mixing time in the recirculation zone is measured using various obstructions by the sodium D-line emission method [20]. A fine-mist spray of a saturated NaCl-aqueous solution is injected impulsively (duration: 1 s) into the air supply plenum before a honeycomb flow straightener using an artist's airbrush. The impulsive injection used for the aqueous solution and the agent is identical in principle. The emission of sodium D-lines (589.0 nm and 589.6 nm) by flame reactions in the high-temperature recirculation zone is col-

lected by a lens (51-mm-dia., f8), passed through an interference filter (589 nm, full width half maximum [FWHM]: 10 nm), and detected by a photomultiplier. The converted electronic signal is conditioned by a low-pass filter (typically 20-Hz cutoff frequency) and an amplifier. The sodium emission intensity saturates at a maximum value during the pulsed injection period and then decays. By assuming that the recirculation zone behaves as a perfectly stirred reactor, with entrainment from and discharge to the free airstream, seeded with a specific species, the first-order differential equation for the mole fraction ( $X$ ) of the species in the recirculation zone is

$$X = -\tau(dX/dt) \quad (1)$$

where  $t$  is the elapsed time, and  $\tau$  is the characteristic mixing time. The solution for the equation describing decay in response to a falling step function ( $X_0 \rightarrow 0$ ) is

$$(X/X_0) = \exp(-t/\tau) \quad (2)$$

where  $X_0$  is the initial mole fraction of the seed species. By assuming that the measured sodium emission intensity ( $I$ ) is proportional to  $X$ , a slope of the decay in a  $\ln(I/I_0)$  vs.  $t$  plot becomes  $-1/\tau$  where  $I_0$  is the initial intensity. The mean characteristic mixing (or residence) time ( $\tau_{\text{exp}}$ ) in the recirculation zone is determined from the mean sodium emission intensity obtained by averaging approximately 200 measurements.

## RESULTS AND DISCUSSION

### Flame Stabilization and Suppression Regimes

Figure 3 shows conceptual schematics of step-stabilized nonpremixed methane flames. As the air velocity was increased, two distinct flame stabilization and suppression regimes were observed: rim-attached (regime I) and wake-stabilized (regime II). In regime I at low air velocities at the step ( $U_{\text{as}} < \text{approximately } 3 \text{ m/s}$ ), a wrinkled laminar diffusion flame attached to the rim of the backward-facing step and developed in the shear layer downstream. There existed a short ( $\sim 2 \text{ cm}$ ) blue flame zone, with a dark space ( $\sim 1 \text{ mm}$ ) between the flame base and the

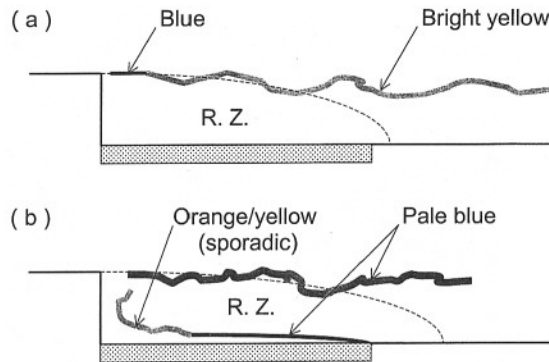


Fig. 3. Flame stabilization and suppression regimes of methane flames; (a) regime I: rim-attached flame, (b) regime II: wake-stabilized flame. R. Z.: recirculation zone.

rim, and a long ( $\sim 50$  cm) trailing bright-yellow flame, typical of hydrocarbon diffusion flames. The video images, with a short shutter speed ( $1/10,000$  s), clearly showed the wrinkled laminar flame structure of the trailing turbulent flame, generated as a result of the interaction of the flame zone with large-scale vortices developed in the shear layer. In regime I, the flame attachment defined the initial condition before the agent injection; the oxygen was prevented from penetrating the fuel side of the flame and thus the recirculation zone was filled mostly with the fuel and products. The oxygen leakage through a relatively low-strain diffusion flame is typically  $\sim 2\%$  [21]. As a pulse of the agent arrived at the test section, the flame base immediately detached from the rim, drifted downstream past the nonflammable recirculation zone, and eventually blew out. If sufficient fuel-air mixing occurred downstream as the agent pulse passed by before blowout, the flame could propagate back through the boundary layer along the bottom surface of the test section and reattach to the rim. Therefore, in regime I, the suppression limit depended on the fuel-air mixing and propagation of partially premixed flame downstream of the recirculation zone.

On the other hand, in regime II, at high mean air velocities at the step, combustion processes occurred in two major regions: the shear layer and the recirculation zone. In the shear layer, a turbulent blue flame was held approximately 1 cm downstream of the rim (analogous to lifted turbulent jet diffusion flames). In the recircula-

tion zone, a blue flame with sporadic orange/yellow flashes was stabilized. Apparently, packets of air were entrained dynamically into the recirculation zone through the turbulent flame in the shear layer and formed a diffusion flame over the porous plate. Therefore, the initial conditions before the agent injection were markedly different from those in regime I. In regime II, the agent-laden air packets could also be entrained into the recirculation zone. It is notable that as the step height was increased, the flow in the wake appeared to become more three-dimensional; there was a main recirculating flow in the central region along the wind tunnel axis, approaching the step and turning outward toward the side windows, and a reversing corner vortex in the inner corner of the step. In the transition region from regimes I to II, at moderate mean air velocities, a highly unstationary flame was observed with the flame base moving back and forth (5–15 cm from the step).

Figures 4 through 6 show the instantaneous schlieren photographs (partial views) of methane flames behind a 32-mm step at the event of suppression under three different inlet air velocities ( $U_{a0} = 1.4, 2.9,$  and  $7.1$  m/s) in regime I, transition, and regime II, respectively. The agent was released into the airflow for a duration of 0.25 s for all cases. Because of the knife-edge of the schlieren system was placed vertical, the image showed the horizontal gradient of the refractive index field, which depended primarily on the density and, thus, the temperature in the flame. In addition, the schlieren deflectometry was able to capture the wave of agent-laden airflow as fine irregularity due to the agent's high molecular weight (149).

In a rim-attached flame in regime I (Fig. 4a), the time-exposure ( $1/125$  s) image of the luminous (yellow) flame in the shear layer was also recorded along the extension of the upper surface of the step. Although the aforementioned three-dimensional motion existed in the recirculation zone and wavy flame structure, the line-of-sight schlieren observation visualized the dominantly two-dimensional flame phenomena. At 0.49 s after agent injection (Fig. 4a), the agent arrived in the test section, showing fine irregularity in the airflow. Full-view schlieren photographs (not shown) revealed that the agent dispersed laterally throughout the test

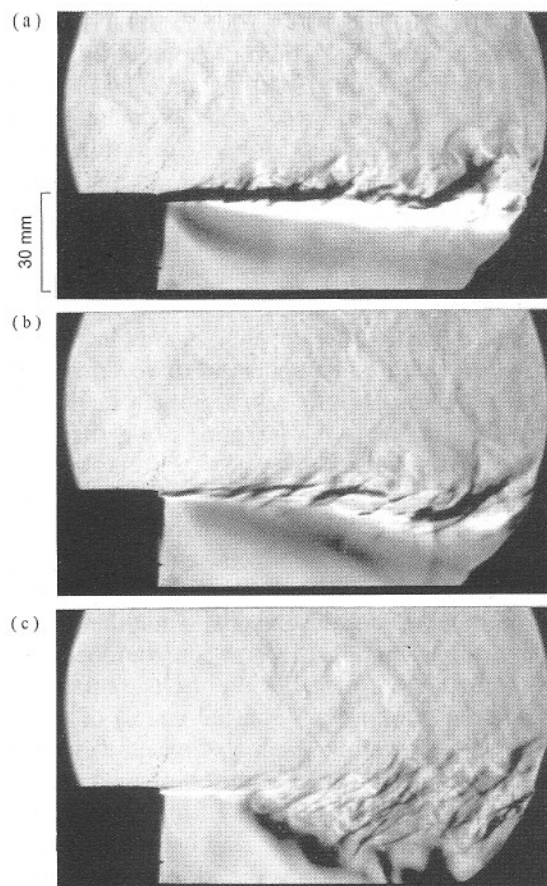


Fig. 4. Schlieren photographs of a rim-attached methane flame (regime I).  $h_s = 32$  mm.  $U_{a0} = 1.4$  m/s. Time after agent injection: (a) 0.49 s, (b) 0.54 s, and (c) 0.63 s. Time of agent arrival:  $\sim 0.49$  s.

section. The hot boundary on the upper side of the flame showed the large-scale vortical nature of the wrinkled flame, while the lower side showed a thick smooth boundary, typical of laminar diffusion flames. At 0.54 s (Fig. 4b), the contrast of the schlieren image near the flame zone became weaker as a result of suppression processes, and the flame base was close to detaching. At 0.63 s (Fig. 4c), the flame base was  $\sim 30$  mm detached from the step, forming a turbulent flame, which was visualized as dark-bright boundaries along the right side of the dark zone in the recirculation zone. The detached flame drifted away further downstream (not shown) and eventually blew out.

In the transition region at a higher inlet air velocity (Fig. 5a), a detached flame showed a large-scale wavy structure in the shear layer and

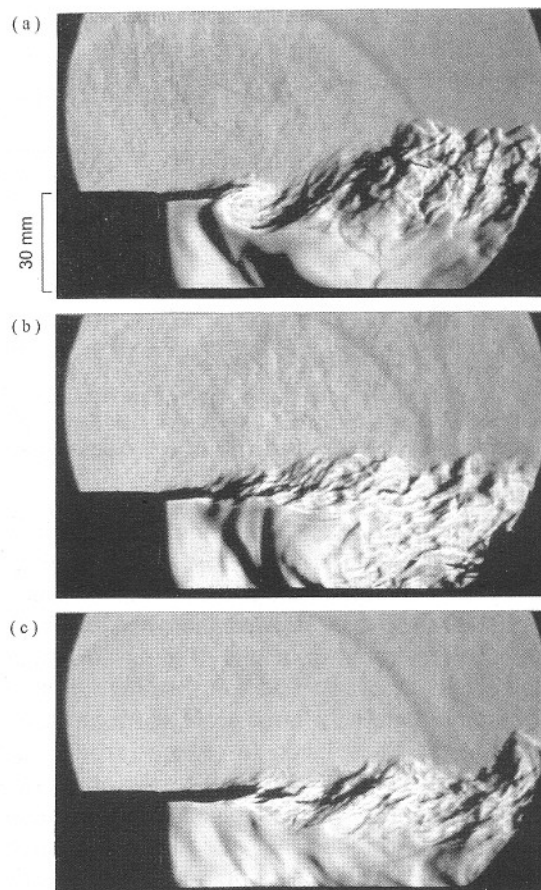


Fig. 5. Schlieren photographs of a transition methane flame.  $h_s = 32$  mm.  $U_{a0} = 2.9$  m/s. Time after agent injection: (a) 0.26 s, (b) 0.29 s, and (c) 0.40 s. Time of agent arrival:  $\sim 0.26$  s.

a separate flame in the recirculation zone along the dark-bright boundaries on the right side of the dark zone, similar to Fig. 4c. The agent arrived in the test section at 0.26 s after injection, showing the irregularity in the left half of the airflow in the image. At 0.29 s (Fig. 5b), the flame zone in the shear layer was affected by the suppressant (lower contrast smaller scale turbulence due to lower temperature), whereas the flame in the recirculation zone was still sustained. At 0.40 s (Fig. 5c), the wake flame was probably extinguished (no dark zone), and the shear layer vortices were visualized by the fuel and the remaining hot gases.

In regime II, at an even higher inlet air velocity (Fig. 6a), a detached turbulent flame was formed in the shear layer, where the small-scale turbulence coexisted with the large-scale

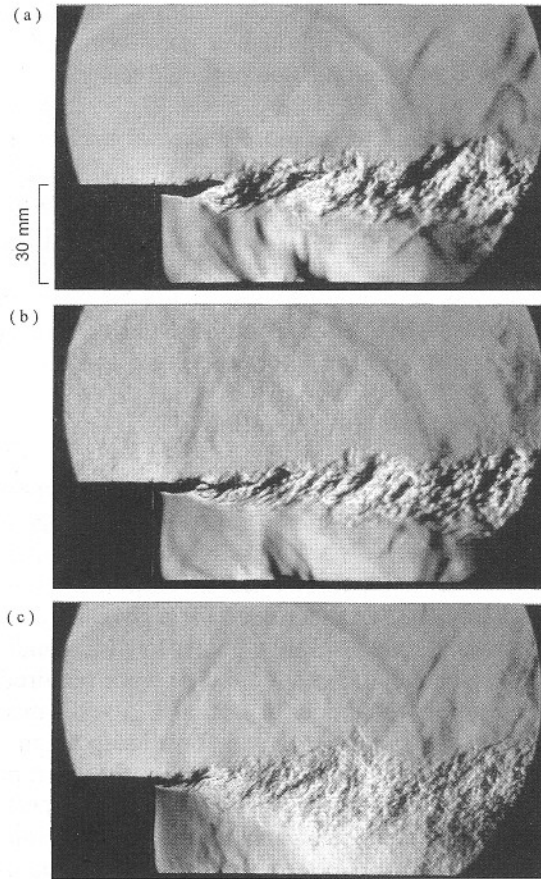


Fig. 6. Schlieren photographs of a wake-stabilized methane flame (regime II).  $h_s = 32$  mm.  $U_{a0} = 7.1$  m/s. Time after agent injection: (a) 0.145 s, (b) 0.15 s, and (c) 0.26 s. Time of agent arrival:  $\sim 0.15$  s.

vortices, and flame elements were also visualized in the recirculation zone. At 0.150 s after injection (Fig. 6b), the agent arrived and the shear layer flame was already affected. At 0.26 s (Fig. 6c), the flame in both shear layer and recirculation zone appeared to be already extinguished, as evidenced by the low-contrast small-scale turbulence in the shear layer and lack of a dark zone in the recirculation zone.

**Characteristic Mixing Time**

Figure 7a shows mean temporal variations of the natural logarithm of the sodium emission intensity normalized by the mean value at saturation for a 64-mm step at various initial mean air velocities. The straight-line part of the decay typically spans two to three orders of magni-

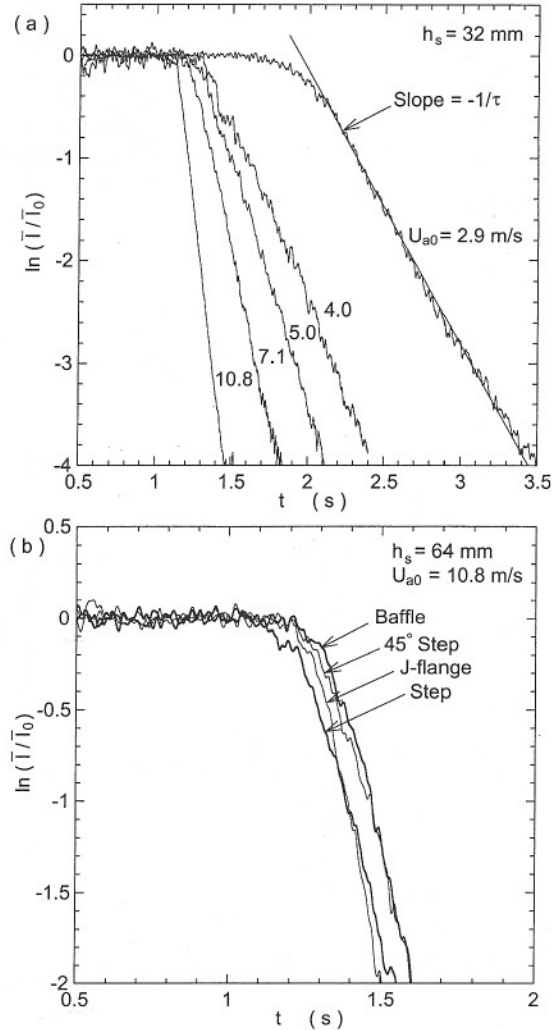


Fig. 7. Temporal traces of the mean sodium D-line emission intensity in the recirculation zone. (a) Effect of the initial mean air velocity. Backward facing step.  $h_s = 32$  mm. (b) Effect of the obstruction geometry.  $h_s = 64$  mm.  $U_{a0} = 10.8$  m/s.

tude. The effect of the obstruction shape on the characteristic mixing time was investigated using obstacles with a height of 64 mm. Figure 7b shows the mean sodium emission intensity for the baffle plate, J-flange, right-angle step, and 45°-angle step. The differences in the curves and their decay slopes are small, indicating that the flow field behind these obstacles is similar. Figure 8a shows the measured characteristic mixing time at various effective mean air velocities for three different step heights. At low effective mean air velocities ( $U_a^* < 3$  m/s) and

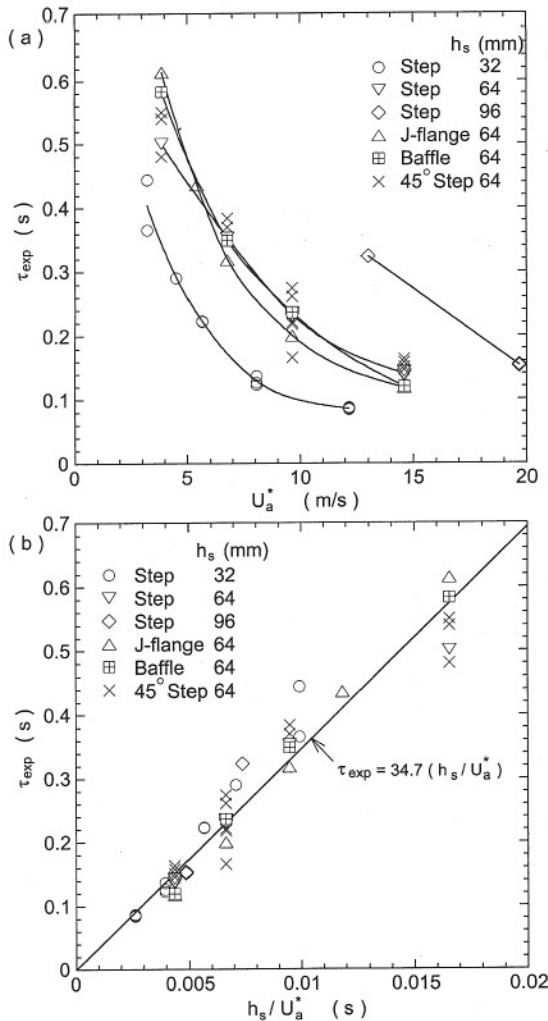


Fig. 8. (a) Measured characteristic mixing time in the recirculation zone behind an obstruction as a function of the effective mean air velocity. (b) Correlation between the characteristic mixing time and the obstruction height normalized by the effective mean air velocity.

long characteristic mixing times ( $\tau_{\text{exp}} > 0.6$  s), the measurement was prohibited because of high-amplitude, low-frequency noises primarily due to temperature fluctuations in the recirculation zone. For a given  $h_s$ ,  $\tau_{\text{exp}}$  decreased monotonically with increasing  $U_a^*$ . For a fixed  $U_a^*$ ,  $\tau_{\text{exp}}$  increased nearly proportionally with  $h_s$ . Thus, the data points of  $\tau_{\text{exp}}$  were replotted against  $h_s/U_a^*$  in Fig. 8b. A fairly good linear correlation (the coefficient of determination  $R^2 = 0.944$ ) was obtained as

$$\tau_{\text{exp}} = 34.7(h_s/U_a^*) \quad (3)$$

in the range of  $3 \text{ m/s} < U_a^* < 20 \text{ m/s}$  and  $0.08 \text{ s} < \tau_{\text{exp}} < 0.6 \text{ s}$ . Although a good correlation ( $R^2 = 0.947$ ) can also be obtained using  $U_{\text{as}}$  as  $\tau_{\text{exp}} = 43.3 (h_s/U_{\text{as}})$  for  $3 \text{ m/s} < U_{\text{as}} < 29 \text{ m/s}$ , Eq. 3 appears to be more universal because it includes the effect of deceleration due to sudden expansion. The correlation equation is simpler than that for an axisymmetric system [20], in which the effect of the blockage ratio is included, probably because of the two-dimensionality, where the step-to-duct distance ratio represents the area (blockage) ratio as well.

### Suppression-Limit Condition

Figure 9 shows the critical agent mole fraction at suppression ( $X_c$ ) as a function of the agent injection period ( $\Delta t$ ) at different mean initial air velocities for three different step heights. In general, as  $\Delta t$  was increased for a given  $U_{a0}$ ,  $X_c$  decreased monotonically. Under low  $U_{a0}$  conditions (regime I), large  $X_c$  and  $\Delta t$  were required to suppress the flame. In fact, at  $U_{a0} = 0.3 \text{ m/s}$ , the suppression limit curves for all step heights exceeded the design criterion for the current halon fire-extinguishing system in the aircraft engine nacelle; i.e., a minimum agent concentration (about 6% by volume) must be maintained throughout the nacelle for a minimum time interval (about 0.5 s) to ensure that the fire will be extinguished and not relight. At low air velocities (regime I), the effect of the step height was weak because the suppression limit was controlled by fuel-air mixing and flame propagation processes downstream of the recirculation zone.

As the agent injection period was increased, the agent mole fraction at suppression approached a minimum value below which no suppression occurred even at long injection periods for all step heights. This minimum agent mole fraction ( $X_c = X_\infty = 0.025$ ) was identical to the value obtained using a counterflow diffusion flame of methane [18] and comparable to the values ( $\sim 0.03$ ) for liquid hydrocarbon fuels (heptane and JP-8) obtained using conventional steady-state cup-burner and counterflow-diffusion-flame methods at relatively low strain rates ( $25\text{--}50 \text{ s}^{-1}$ ) [12–17]. On the other hand, as the agent injection period was decreased, there was a minimum injection period below which the flame could not be extinguished even at high

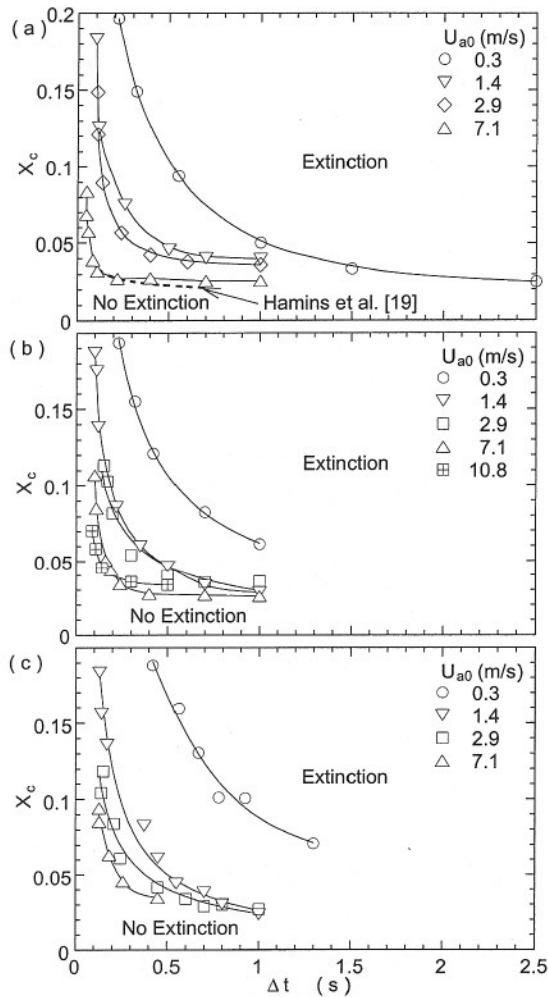


Fig. 9. Measured critical agent mole fraction at suppression as a function of the agent injection period. (a)  $h_s = 32$  mm, (b)  $h_s = 64$  mm, (c)  $h_s = 96$  mm.

agent concentrations. The minimum injection period was nearly proportional to the step height; at  $U_{a0} = 7.1$  m/s,  $\Delta t \approx 0.05$  s for  $h_s = 32$  mm (Fig. 9a),  $\Delta t \approx 0.1$  s for  $h_s = 64$  mm (Fig. 9b), and  $\Delta t \approx 0.15$  s for  $h_s = 96$  mm (Fig. 9c). Surprisingly, the current result for  $h_s = 32$  mm and  $U_{a0} = 7.1$  m/s (Fig. 9a) is close to the suppression limit curve obtained by Hamins et al. [19] for an axisymmetric 35-mm-dia.-baffle-stabilized JP-8 spray flame at the air velocity of 7.5 m/s, although the minimum injection period was not determined in the previous work.

Based on a phenomenological model for a well-stirred reactor developed by Longwell et al. [22], Hamins et al. [19] developed a mixing model

that characterizes the rate of agent entrainment into the recirculation zone. It is assumed that flame extinction occurs when the agent mole fraction in the recirculation zone reaches a critical value ( $X_c$ ) and that complete mixing of the agent in the recirculation zone is instantaneous. By using the first-order differential equation describing mixing in a perfectly stirred reactor, which is identical to Eq. 1, the critical agent mole fraction in the free stream ( $X_c$ ) at extinction is related to the critical agent mole fraction in the free stream for long injection periods ( $X_\infty$ ).

$$X_c = \frac{X_\infty}{1 - e^{(-\Delta t/\tau)}} \quad (4)$$

Hence,  $\tau$  is the characteristic mixing time for entrainment into the recirculation zone. For a long injection period, Eq. 4 becomes  $X_c \approx X_\infty$ . For a short injection period, large free stream agent concentrations are required to obtain extinction. A critical injection period ( $\Delta t_c$ ) below which a flame cannot be extinguished regardless of agent concentration was further derived for  $X_c = 1$ .

$$\Delta t_c = -\tau \ln(1 - X_\infty) \quad (5)$$

For a condition of  $X_\infty = 0.025$  and  $\tau = 0.1$  s, the critical injection period calculated by Eq. 5 becomes  $\Delta t_c = 0.0253\tau = 0.0025$  s. This value is for an idealistic condition at  $X_c = 1$  and much smaller than those of typical of aircraft engine nacelle conditions ( $\sim 1$  s [19]).

Figure 10 shows the suppression limits for regime II and theoretical curves using Eq. 4 with  $X_\infty = 0.025$  and the characteristic mixing time from Eq. 3. The theoretical curves showed the general trend of the experimental results very well and followed the data points fairly well. Therefore, the data points in Fig. 10 are replotted in Fig. 11 in a nondimensional form: the critical agent mole fraction at suppression normalized by the minimum value ( $X_c/X_\infty$ ) vs. the agent injection period normalized by the characteristic mixing time in the recirculation zone ( $\Delta t/\tau_{exp}$ ) with a theoretical curve by Eq. 4. The data points at various mean inlet air velocities for three step heights nearly collapsed into a single curve, thus essentially supporting the physical processes described by Eq. 4. The nondimensional representation of the results revealed that the critical agent mole fraction at suppression dramatically increased as the agent

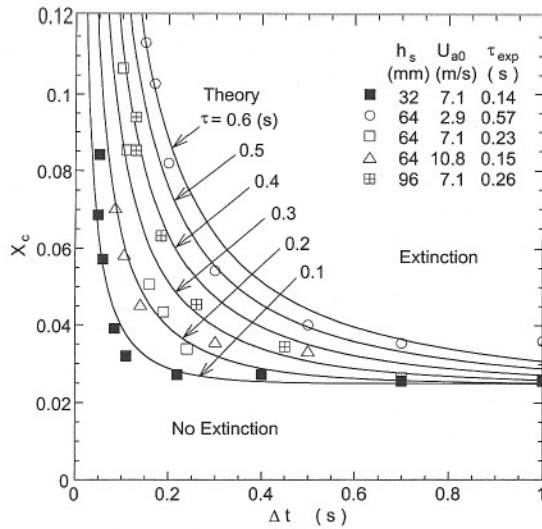


Fig. 10. Measured critical agent mole fraction at suppression and theoretical curves as a function of the agent injection period (regime II).

injection period decreased below the characteristic mixing time. Because the minimum agent mole fraction can be approximated by the value obtained by conventional steady-state methods (i.e., cup-burner or counterflow diffusion flames) and the characteristic mixing time is correlated (Eq. 3) to the experimental conditions (the step

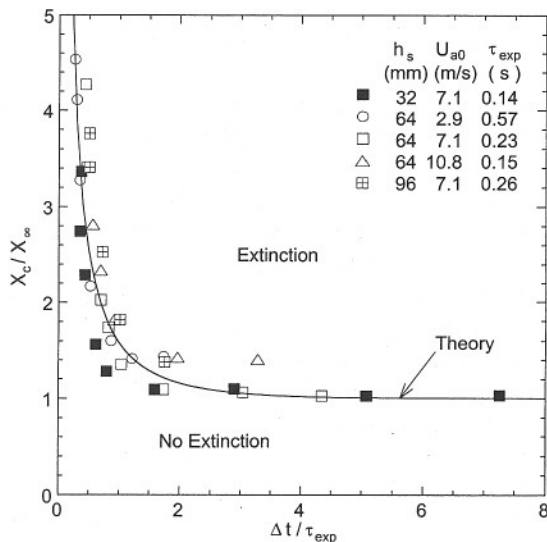


Fig. 11. Measured critical agent mole fraction at suppression normalized by the minimum value at long injection periods and a theoretical curve as a function of the agent injection period normalized by the characteristic mixing time (regime II).

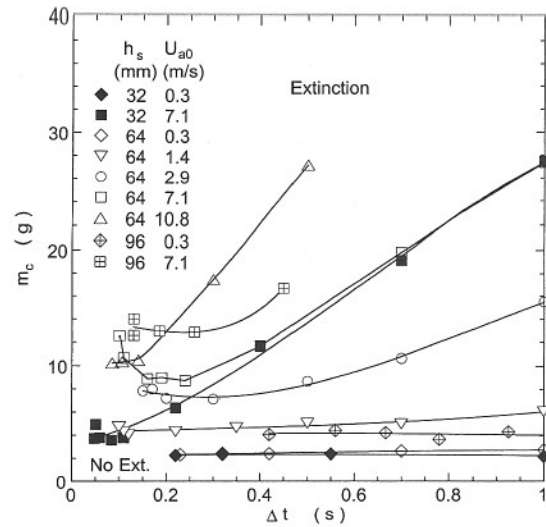


Fig. 12. Measured critical agent mass at suppression as a function of the agent injection period.

height and effective mean air velocity), the suppression limit of step-stabilized flames in regime II can be predicted theoretically.

### Total Agent Mass

From a practical point of view, the total amount of agent required to extinguish fires is important as halon 1301 is replaced with a potentially less effective agent. Figure 12 shows a replot of the suppression-limit data (Fig. 9) expressed in the total agent mass at suppression ( $m_c$ ). At low initial mean air velocities in regime I (see  $U_{a0} = 0.3$  m/s in the figure), the total agent mass at suppression was nearly constant, independent of the agent injection period and mole fraction. At high initial mean air velocities in regime II ( $U_{a0} = 7.1$  and  $10.8$  m/s in the figure), the agent mass at suppression linearly increased with increasing the injection period as  $X_c \rightarrow X_\infty$  and a minimum value existed which increased with the step height. Thus, for regime II, the agent mass at suppression was divided by the step height and plotted against the normalized agent injection period in Fig. 13. The data points tended to lump together, and the minimum points for different step heights and air velocities were in the range of  $m_c/h_s \approx 130 \pm 30$  g/m and  $\Delta t/\tau_{exp} \approx 0.8 \pm 0.2$ . The results indicate that the agent mass per unit step height at suppression was comparable among these conditions and

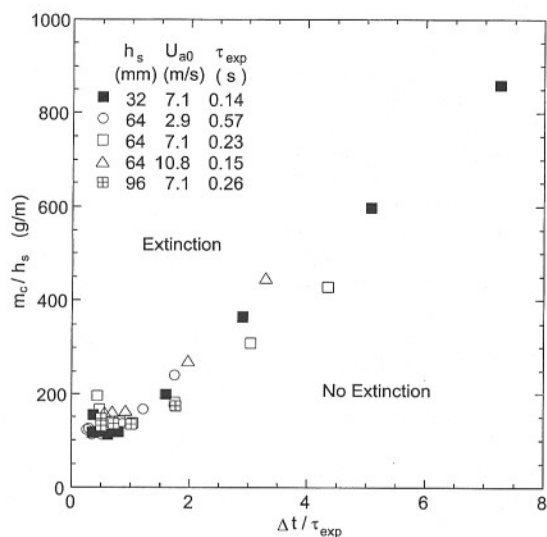


Fig. 13. Measured critical agent mass at suppression divided by the step height as a function of the agent injection period normalized by the characteristic mixing time (regime II).

that the agent mass delivered can be minimized if the injection period is close to the characteristic mixing time in the recirculation zone.

Figure 14 shows the minimum total agent mass ( $m_{c,min}$ ) determined from the minimum values in both regimes I and II, plotted against the initial mean air velocity with the flame detachment con-

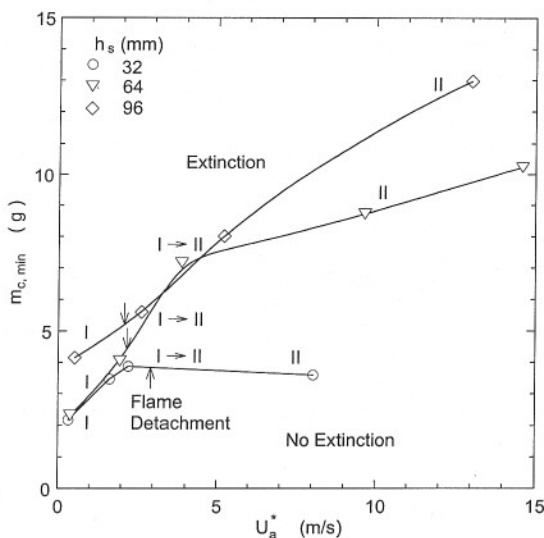


Fig. 14. Measured minimum critical agent mass at suppression as a function of the effective mean air velocity with corresponding flame stabilization and suppression regimes.

ditions and corresponding regimes. As  $U_{a0}$  was increased,  $m_{c,min}$  increased proportionally in regime I, and the curves tended to level off as the transition to regime II occurred. A larger step possessing a larger recirculation zone volume requires a larger agent mass to achieve the same agent concentration in the recirculation zone to extinguish the flame.

### Suppression Mechanism

The extinction of diffusion flames is generally explained [23] by a critical Damköhler number ( $Da = \tau_r/\tau_c$ ,  $\tau_c$ : the chemical time, and  $\tau_r$ : the flow or diffusion time) below which extinction occurs. Because halon 1301 is considered as mostly chemical suppressant with some thermal effects, increasing the agent concentration enhances chemical inhibition (and heat losses), thus increasing the chemical time and decreasing  $Da$  down to the critical value. The current results revealed that  $X_\infty$  was comparable to the values obtained by the steady-state cup-burner or low-strain-rate counterflow diffusion flame, that the dependence of  $X_\infty$  on the airflow velocity is small, and that suppression occurred if the agent injection period was long enough to increase the agent mole fraction in the recirculation zone to  $X_\infty$ . In addition, even at high air velocities in regime II, there exists the relatively low-strain flame in the low-velocity recirculation zone besides the high-strain flame in the shear layer. Therefore, the suppression of step-stabilized flames appears to occur under the extinction condition of relatively low-strain-rate diffusion flames. Although the experimental conditions of the data presented here are limited, the basic concept for suppression criterion obtained for a gaseous fuel using a simple geometry must be applicable to a liquid-fuel pool fire stabilized in more complex clutter configurations.

### CONCLUSIONS

The suppression limits of nonpremixed methane flames stabilized by a backward-facing step in an airstream were measured as the critical agent mole fraction at suppression by varying the unsteady injection period of a gaseous fire-extinguishing agent ( $CF_3Br$ ) for various air velocities and three step heights. The behavior of

flame suppression was affected by two distinct flame stabilization regimes: rim-attached (regime I) and wake-stabilized (regime II). The suppression in regime I occurs as the detached flame in the shear layer blows out, whereas the suppression in regime II took place as the flames in the shear layer and the recirculation zone extinguish consecutively. The measured suppression-limit data points in regime II collapsed into a single curve when plotting the critical agent mole fraction at suppression normalized by its minimum value (0.025) obtained at long injection periods as a function of the agent injection period normalized by the measured characteristic mixing (residence) time. Because the minimum value is identical to the value obtained for a low strain-rate counter-flow diffusion flame, the suppression in regime II must be controlled by the low strain-rate flame in the low-speed recirculation zone even at high free-stream velocities. The data trend can be predicted by a theoretical expression using the measured characteristic mixing time. The agent mass delivered can be minimized by injecting the agent for a period near the characteristic mixing time. The minimum agent mass required to extinguish the flame increases with the volume of the recirculation zone.

*This research is part of the Department of Defense's Next-Generation Fire Suppression Technology Program, funded by the DoD Strategic Environmental Research and Development Program and the Air Force Research Laboratory, Propulsion Directorate, Propulsion Sciences and Advanced Concept Division, Wright-Patterson Air Force Base, Ohio, under Contract No. F33615-97-C-2719 (Technical Monitor: C. W. Frayne).*

## REFERENCES

1. *Report of the Halon Fire Extinguishing Agents Technical Options Committee*, United Nations Environment Programme (UNEP), 1994.
2. Lefebvre, A. H., *Gas Turbine Combustion*, Hemisphere, New York, 1983, p. 179.
3. Raghunandan, B. N., and Yogesh, G. P., *Twenty-Second Symposium (International) on Combustion*, The Combustion Institute, Pittsburgh, 1989, p. 1501.
4. Rohmat, T. A., Katoh, H., Obara, T., Yoshihashi, T., and Ohyagi, S., *ALAA J.* 36:1945 (1998).
5. Hirst, R., Farenden, P. J., and Simmons, R. F., *Fire Technol.* 12:266 (1976).
6. Hirst, R., Farenden, P. J., and Simmons, R. F., *Fire Technol.* 13:59 (1977).
7. Dyer, J. H., Marjoram, M. J., and Simmons, R. F., *Fire Technol.* 13:126 (1977).
8. Dyer, J. H., Marjoram, M. J., and Simmons, R. F., *Fire Technol.* 13:223 (1977).
9. Moussa, N. A. (1994). *Effects of Clutter on Performance of Fire Suppression Agents in Aircraft Dry Bays and Engine Nacelles*, Report prepared for Booz, Allen and Hamilton, Dayton, OH.
10. Grosshandler, W. L., Gann, R. G., and Pitts, W. M., in *Evaluation of Alternative In-Flight Fire Suppressants for Full-Scale Testing in Simulated Aircraft Engine Nacelles and Dry Bays* (W. L. Grosshandler, R. G. Gann, and W. M. Pitts, Eds.), National Institute of Standards and Technology, Gaithersburg, MD NIST SP 861, 1994, p. 1.
11. Hamins, A., Cleary, T., Borthwick, P., Gorchkov, N., McGrattan, K., Forney, G., Grosshandler, W., Presser, C., and Melton, L., in *Fire Suppression System Performance of Alternative Agents in Aircraft Engine and Dry Bay Laboratory Simulations, Vol. II*, (R. G. Gann, Ed.), National Institute of Standards and Technology, Gaithersburg, MD, NIST SP 890, 1995, p. 1.
12. *Standard on Clean Agent Fire Extinguishing Systems*, National Fire Protection Agency, NFPA 2001, 1988.
13. Hamins, A., Gmurczyk, G., Grosshandler, W., Rehwooldt, R. G., Vazquez, I., Cleary, T., Presser, C., and Seshadri, K., in *Evaluation of Alternative In-Flight Fire Suppressants for Full-Scale Testing in Simulated Aircraft Engine Nacelles and Dry Bays* (W. L. Grosshandler, R. G. Gann, and W. M. Pitts, Eds.), National Institute of Standards and Technology, Gaithersburg, MD, NIST SP 861, 1994, p. 345.
14. Hamins, A., Trees, D., Seshadri, K., and Chelliah, H. K., *Combust. Flame* 99:221 (1994).
15. Sakai, R., Saito, N., Saso, Y., Ogawa, Y., and Inoue, Y. (1995). *Flame Extinguishing Concentrations of Halon Replacements for Flammable Liquids*, Report of Fire Research Institute of Japan, No. 80, p. 36.
16. Saito, N., Ogawa, Y., Saso, Y., and Sakai, R. (1996). *Improvement on Reproducibility of Flame Extinguishing Concentration Measured by Cup Burner Method*, Report of Fire Research Institute of Japan, No. 81, p. 22.
17. Saso, Y., Saito, N., Liao, C., and Ogawa, Y., *Fire Safety J.* 26:303 (1996).
18. Papas, P., Fleming, J. W., and Sheinson, R. S., *Twenty-Sixth Symposium (International) on Combustion*, The Combustion Institute, Pittsburgh, 1996, p. 1405.
19. Hamins, A., Presser, C., and Melton, L., *Twenty-Sixth Symposium (International) on Combustion*, The Combustion Institute, Pittsburgh, 1996, p. 1413.
20. Winterfeld, G., *Tenth Symposium (International) on Combustion*, The Combustion Institute, Pittsburgh, 1965, p. 1265.
21. Tsuji, H., and Yamaoka, I., *Thirteenth Symposium (International) on Combustion*, The Combustion Institute, Pittsburgh, 1971, p. 979.
22. Longwell, J. P., Frost, E. E., and Weiss, M. A., *Indust. Engin. Chem.* 45:1629 (1953).
23. Williams, F. A., *J. Fire Flammability* 5:54 (1974).

*Received 22 February 1999; revised 8 November 1999; accepted 5 January 2000*